RESEARCH   **Open Access**

A composite method for improving the resolution of passive radar target recognition based on WiFi signals

Xiaokun Zheng[1,2*†] ⓘ, Ting Jiang[1†] and Wenling Xue[1,2]

Abstract

To improve the resolution of passive radar target recognition based on WiFi signals, a composite preamble scheme is proposed. In addition, a composite approach combined with cancelation and decomposition in an interior scenario is studied. With this method, short sensing signals, such as chirps with no extra bandwidth, are overlayed onto a long WiFi preamble (802.11a) in the time domain. After detection and coarse sync using the short preamble at the Rx side, most of the chirp signal is removed prior to fine channel estimation (CE). Although the slight influence on CE may cause a fractional increase in the relative constellation error, the method can obtain a higher communication performance than normal multiplex integration. Finite-difference time-domain (FDTD) simulations show that when the same time-domain features are extracted, the composite signal provides a better recognition effect than when only using the WiFi preamble. The method is useful for health care such as elderly toilet/bathroom standing/lying detection, or device-free people counting.

Keywords: Recognition method, Improve correctness, WiFi, Composite signal

1 Introduction

The Internet of Things (IOT) is being propelled by the convergence of sensing, communication, computing, and control. Integrated smart sensing and communication is a hot issue for communication terminals. It is important in the fields of health care, military, transportation [1], industrial monitoring, border patrol, etc. The key to signal integration is to design a waveform that simultaneously provides the functionalities of communication and sensing.

Traditional radar technology, such as bistatic radar [2], was initially used for smart sensing. Then, in [3, 4], WiFi signals were used for human fall detection and gesture recognition, [3] reported 87% or 90% fall detection accuracy when magnitude of CSI or the phase difference across multiple antennas was used, and [5, 6] discussed multistatic passive radar using WiMAX and RFID; however,

their sensing resolutions were generally relatively limited. Yu Guo, Usman Mahmood, Zhong et al. [7–9] used deep learning/SVM classification based on privileged information or fourth-order cumulant to improve recognition correctness. On the other hand, to achieve higher resolution, certain signals suitable for sensing have been used to recognize and transmit data simultaneously. For example, LFM-MSK or FMCW [10] based on chirp signals, are used for integrated systems with relatively low data rates; in [11], pulse waveform OFDM was used for high-resolution detection, although its synchronization is costly.

Various multiplexing-based methods, such as time [1], frequency [12], code [13], and spatial-division multiplex integration [14], have also been proposed, whereby both data rate and sensing resolution can achieve a relatively high performance. Moreover, cancelation technology is used to reduce interference between the sensing carrier and the transfer sub-carrier in MIMO-OFDM integrated systems [15]. Mark Roberton proposed a chirp spread-spectrum signal [16], with the help of de-spreading to reduce mutual interference.Then long pseudo random code is generally needed and data rate is affected. In [17], CP-based OFDM high-resolution imaging, which requires

*Correspondence: 1053072637@qq.com
†Xiaokun Zheng and Ting Jiang contributed equally to this work.
[1]Key Labs of Universal Wireless Communications, Beijing University of Posts and Telecommunications, 100876 Beijing, China
[2]College of Electronics Information and Engineering, Hebei University, Wusi East Road, 071002 Baoding, China

a sufficient cyclic prefix, was proposed. Multiplex mode generally requires more resources.

A composite integration is proposed in this paper. Our main contributions are as follows. (1) A composite preamble scheme is proposed to improve the target recognition resolution of passive radar using WiFi. Thereby, a higher communication performance than normal multiplex integration can be obtained. The composition can only be applied at the Tx side. It can also be applied at both the Tx and Rx sides, which means that the preamble at the Tx and Rx sides can be replaced by the same composite preamble simultaneously. (2) The synthesis can be in the time domain, or in the frequency domain which possesses good autocorrelation, anti-fading performance and sharper ambiguity function. Thus, the channel estimation of the long preamble is retained, and its recognition resolution is improved. (3) In this paper, a time-domain composite at the Tx side combined with cancelation and decomposition is studied. We verified that the method can improve the resolution of object recognition for interior scenes. The scene can be empty; it can also include some fixed arrangement. And we are adding more pertinent recognition test for application-specific scenario; we will also focus on applying suitable composite(such as f-domain composite) preamble at both the Tx and Rx sides next; there would then be no need to consider the effects of deletion and residues.

In this paper, we emphasize the time domain. The waveform of the data section varies with the transmitted data, and it is rather complex for use in recognition tasks [4]. Thus, we use the preamble, and a short sensing signal, such a chirp with no extra bandwidth, is overlaid onto the long preamble of 802.11a WiFi [18]. After detection and coarse sync at the Rx side, the pre-process or pre-fade chirp signal is removed according to $k \cdot T_{step}$ based on the coarse sync and using a parallel correlator [19, 20]. Here, T_{step} is the delay increment step, $k = 0, 1, 2....$. Then, the residual jamming signal is decomposed when the long preamble makes correlation with many corresponding delays local sequences (Fig. 2b). OFDM can be used to transfer data at high speed in the data section, and the sensing part is easy to extract. A small constant-amplitude overlapping chirp at the transmitter has a minimal effect on the peak-to-average-power ratio (PAPR). The power of the overlapping signal can be easily adjusted according to the sensing precision and CE precision, and the system change is smaller than time multiplex integration [1]. The FDTD simulation shows that the composite signal provides better recognition performance than simply using the WiFi preamble. Although there is a slight influence on frequency offset (FO) estimation and frequency-domain equalization (FDE) [21], which may cause a fractional increase in the relative constellation error (RCE) [18], the method still has a relatively high data transmission

capacity. The method is useful for device-free people counting [22] at the entrance, such as making a distinction between adults and children. And it is useful for fall detection in toilet/bathroom, etc, such as there was a nearly 100% human standing/lying recognition accuracy in the simulation in this paper when preamble signal was used.

The remainder of this paper is organized as follows. The scheme of the signal composite integration is introduced in Section 2. The principle and scheme of the separation method are introduced in Section 3. Section 4 presents the FDTD-based simulation results and discussion. The conclusion is provided in Section 5.

2 Methods of the composition

To improve the recognition resolution of WiFi signals and reduce the impact on communication, a short sensing signal is overlaid onto its long preamble, with neither extra bandwidth nor time slots required, as shown in Fig. 1. The data section varies with the transmitted data; it is too complex to be used for recognition [5]. Therefore, we use the preamble. The duration or power of the overlapping can be adjusted.
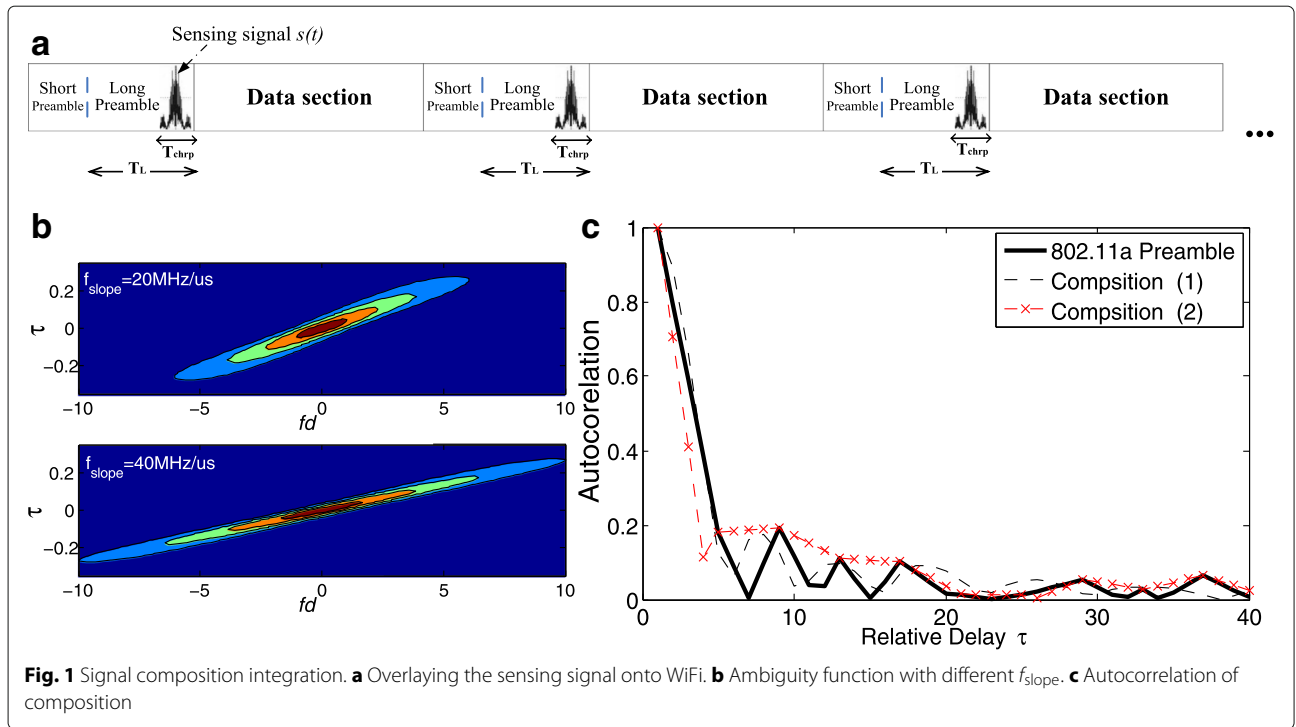
The composite preamble signal is expressed as (1, 2), where $La(t)$ is time domain of the 802.11a long preamble, L is frequency-domain, $L = \{00000, 1, 1, -1 \ldots 1, 1, 000000\}$ and $La(t) = \sum_k L_k \cdot exp(j2\pi k \Delta_F t) = IFFT(L)$ [18]. s(t) is the short sensing signal, T_L and T_{chrp} are the duration times of La(t) and s(t), respectively.

$$P_r(t) = \begin{cases} L_a(t) & 0 \le t \le T_L - T_{chrp} \\ L_a(t) + s(t) & T_L - T_{chrp} < t \le T_L \\ 0 & else \end{cases} \quad (1)$$

$$P_{rr}(t) = IFFT[L + k_s \cdot abs(FFT(s(t)))] \quad (2)$$

Figure 1c shows that both of the compositions have good autocorrelation. However, for the reason that the overlaid signal is an envelope signal, anti-fading performance of composition (1) is slightly worse when CE is performed, (1) is not quite suitable for replacing original preamble at both Tx and Rx sides directly. So in this paper, we emphasize the time-domain composition at Tx side; and the sensing signal $s(t)$ is removed and decomposed at Rx side. Composition in f-domain (2) will be researched next.

Here, we select a chirp as the sensing signal, and we use the composite fragment $L_a(t) + s(t)$ for recognition. $s(t)$ can be expressed as $s(t) = U(t)e^{-j2\pi t\left(f_0 + \frac{1}{2}f_{slope} \cdot t\right)}$, where f_{slope} is the slope and U(t) is the roughly constant envelope pulse in this paper. If the power of the chirp P_{chrp} is less than 1.2 times the long preamble P_L, recognition correctness will not increase noticeably (Fig. 4a); therefore, P_{chrp} should be $> 1.2P_L$. On the other hand, if P_{chrp} is too large, it will seriously affect the fine FO estimation or RCE. For example, when $P_{chrp} > 2P_L$, the FO estimation

Zheng *et al. EURASIP Journal on Wireless Communications and Networking* (2018) 2018:215

Page 3 of 12

Fig. 1 Signal composition integration. **a** Overlaying the sensing signal onto WiFi. **b** Ambiguity function with different f_{slope}. **c** Autocorrelation of composition

correctness will greatly decrease, and FDE cannot be completed (see Figs. 4b and 7a). Moreover, when $P_{\text{chrp}} = 2P_L$, a satisfactory increase in the recognition correctness can be obtained (Fig. 9). Thus, $1.2P_L < P_{\text{chrp}} \leq 2P_L$ is recommended.

With the same power P_{chrp}, a longer T_{chrp} results in a more serious influence on FO estimation and FDE. In the case of $P_{\text{chrp}} = 1.2P_L$, when Ts = 1 us, the correctness will greatly decrease as well (Fig. 4b). Thus, P_{chrp} cannot be smaller, and therefore, Ts1 us is required. On the other hand, if T_{chrp} is too short, an insufficient number of sample points will be obtained, and the recognition task will not be performed accurately. As described by the USRP (Universal Software Radio peripheral) data sheet [23], if we set the front-end sample rate as f_s = 200 MHz and T_{chrp} < 0.25 us, < 50 sample points can be used for recognition, which cannot achieve complete complex recognition. In addition, considering that general radar signal processing boards support higher f_s, we emphasize f_s = 200 and 400 MHz and Ts = 0.5 us in the FDTD simulation in this paper.

With the same duration and bandwidth, f_{slope} of the chirp signal modulated with single-side band (SSB) technology could have a greater value than DSB. 802.11a uses a bandwidth of 20 MHz [18]; when the chirp signal is modulated with DSB, its f_{slope} can be less than approximately 20 MHz/us (here, Ts = 0.5 us). Then, it would occupy a bandwidth of less than 20 MHz. On the other hand, when modulated with SSB, its frequency change rate f_{slope} can

be less than approximately 40 MHz/us. Equation (3) is the ambiguity function of the chirp signal [24]. We can see that a larger f_{slope} results in a more pronounced spike and higher resolution. Figure 1b shows the ambiguity function with different f_{slope} without extra bandwidth.
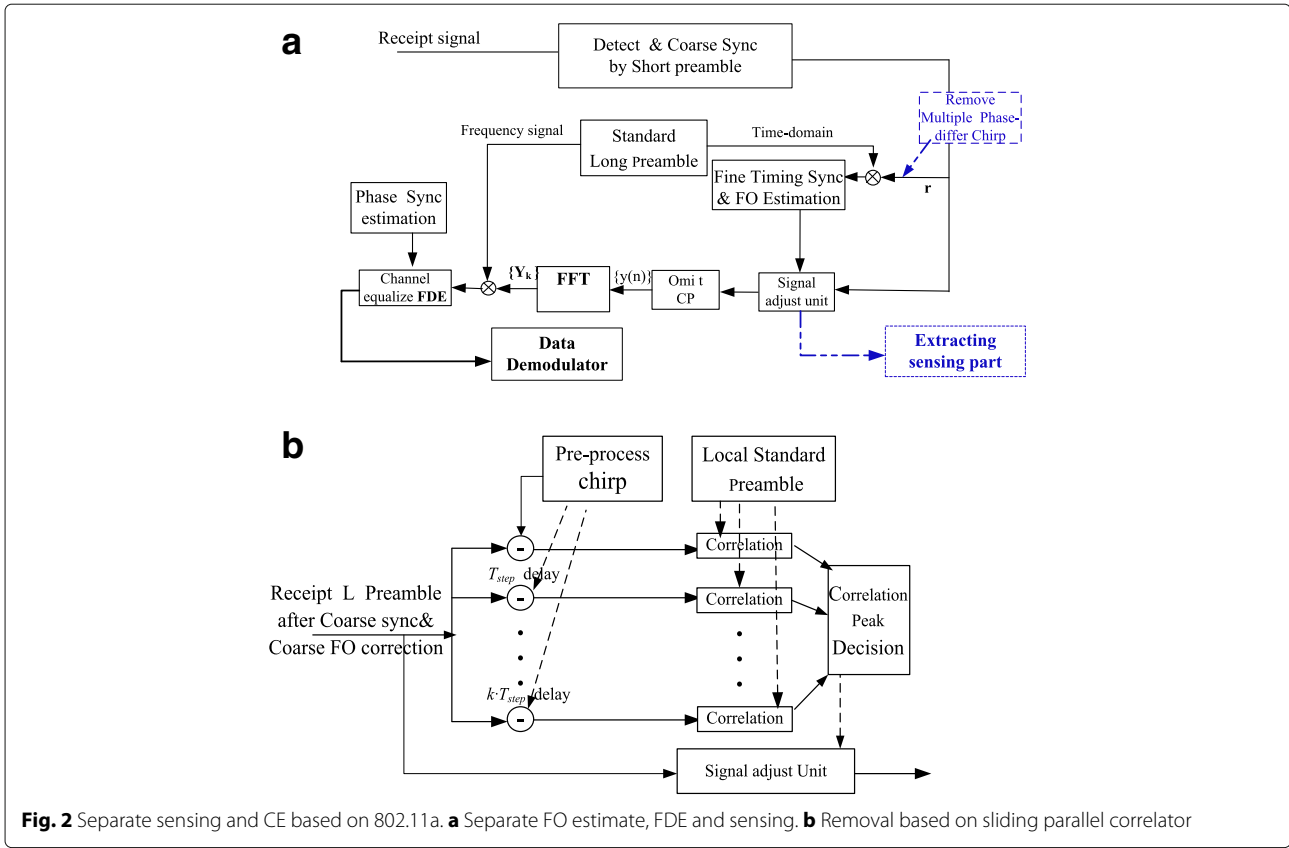
$$|x(\tau, f_d)|^2 = \begin{cases} \left|(T_{\text{chrp}} - |\tau|) \cdot \sin c((f_d - f_{\text{slope}}\tau)(T_{\text{chrp}} - |\tau|))\right|^2 & |\tau| < T_{\text{chrp}} \\ 0 & \text{else} \end{cases}$$

(3)

3 Methods of cancelation and decomposition

The composite signal can be used for recognition. In addition, when channel estimation (CE) is performed, the chirp signal should be removed. Figure 2 shows the scheme for extracting the sensing part and the scheme for removing when CE. After detection and coarse sync by the short preamble at the Rx side, the pre-process chirp is removed according to $k \cdot T_{\text{step}}$ based on both the coarse sync ($k = 0, 1, 2, \ldots$) and the sliding parallel correlator [20, 21, 25]. Then, the residual jamming is decomposed when the long preamble makes a correlation with local sequence and makes FFT for FDE.

3.1 Removing overlapped signal

To guarantee the channel estimation performance of the synthesis preamble, before being correlated with multiple delay-different $k \cdot T_{\text{step}}$ local sequences, the corresponding phase chirp is removed according to $k \cdot T_{\text{step}}$ based on the coarse sync ($k = 0, 1, 2, \ldots$). Here, we use a sliding parallel

Fig. 2 Separate sensing and CE based on 802.11a. **a** Separate FO estimate, FDE and sensing. **b** Removal based on sliding parallel correlator

correlator to fine tune the sync. Based on the coarse sync, parallel correlators do not require too many resources. In addition to the chirp signal on the Tx side, it can be considered for removing pre-fade or pre-processing the chirp signal. Here, the pre-processed signal is defined as

$$S_{pre}(f) = H(f) \cdot S(f) + N_i(f) \tag{4}$$

where $S(f)$ is the chirp signal on the Tx side, and $H(f)$ is the transfer function of the interior scene without the sensing object and no people (It can be empty or include some fixed arrangement). $S_{pre}(f)$ can be recorded in advance for a given scenario, where the locations of the transmitter and receiver are fixed and there are neither sensing objects nor people. The interior scene could be viewed as a waveguide; we use the FDTD method [26, 27] to achieve accurate computation.

The insertion of the sensing object will cause a disturbance in the electric field distribution. Let $H'(f)$ denote the new transfer function, and the received signal is $Sr(f)$. Then,

$$S_r(f) = H'(f) \cdot S(f) + N_i(f) \tag{5}$$

After removing the sending $S(f)$ or pre-processed $S_{pre}(f)$, the remainder are $S_{rest}(f)$ or $S_{p,rest}(f)$, respectively:

$$S_{rest}(f) = [H(f) - 1] \cdot S(f) + N_i(f), \quad and \tag{6}$$
$$S_{p\_rest}(f) = [H(f) - H'(f)] \cdot S(f) + [N_i(f) - N(f)]$$

In real applications, $S_{rest}(f)$, $S_{p\_rest}(f)$ or their mean value can be measured; they can then be compared to decide which should be removed. In this paper, the sensing objects are mainly hollow balls with diameters of 21 cm and 22 cm, the disturbance is small, and we select pre-processed signals for removal in our simulation test.

Figure 3 shows the $S_{pre}(f)$ and $S_r(f)$ signals recorded by the recorder of the FDTD simulation; here, after the FDTD calculation, we introduce noise with an SNR of 6.5 dB. In addition, when we perform FO estimation, FDE and recognition tests, [−4∼16 dB] SNRs are considered in Figs. 4, 9, and 10. The dotted line represents $S_{pre}(f)$, and the solid line represents $Sr(f)$ with the object. We can see the difference caused by the insertion of the sensing object. Table 1 shows the removal of the residue in our study.

There are certain requirements on the front-end sample rate at the Rx side. Considering the 20 MHz bandwidth limit of 802.11a WiFi, see Table 1 for the main parameters of the chirp overlapping and removal in our study.
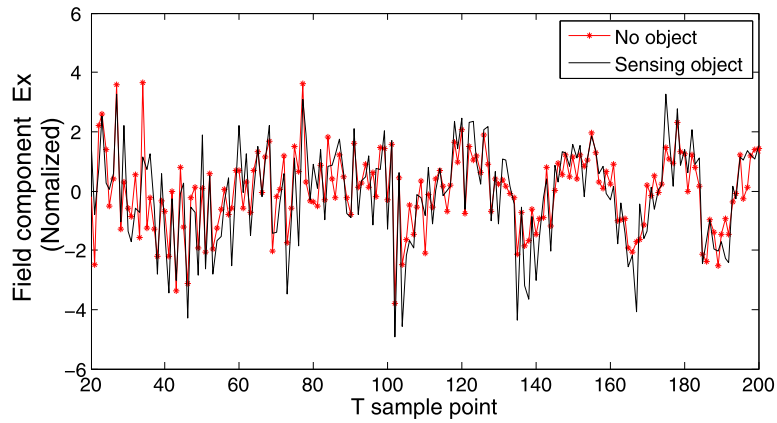
Zheng *et al. EURASIP Journal on Wireless Communications and Networking*   (2018) 2018:215

Page 5 of 12

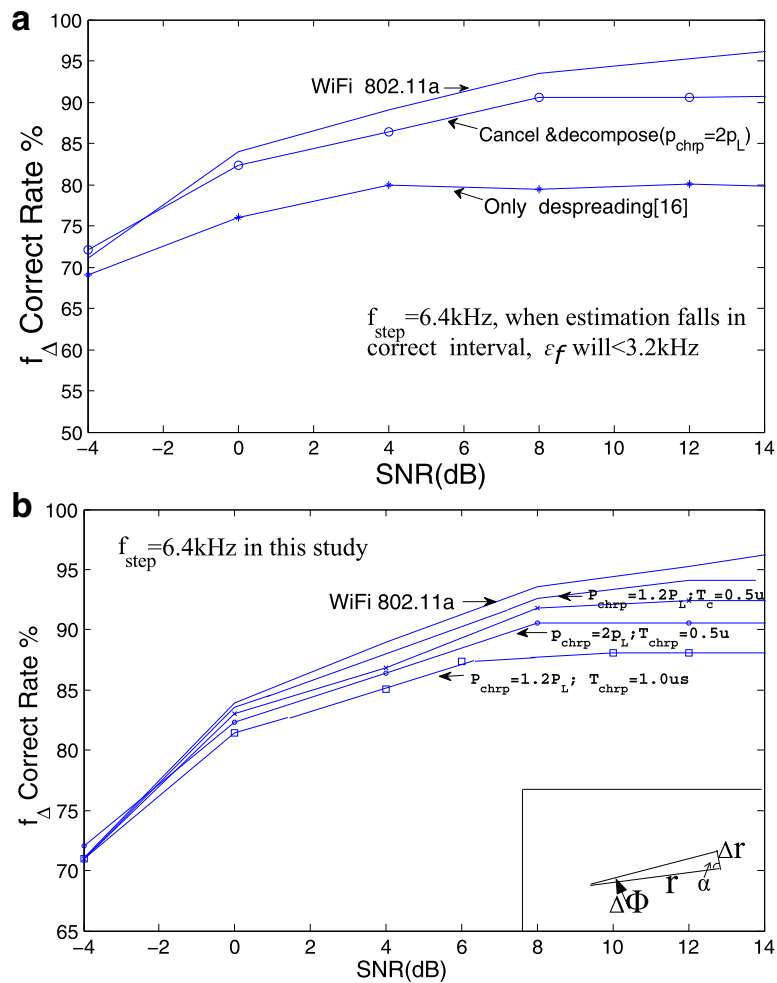**Fig. 3** Difference in received signal caused by sensed object

Fig. 4 Frequency offset estimation result. **a** Canceling and decomposing vs. only de-spreading. **b** Powers of chirps overlapped are different

Table 1 Residue vs. sync precision

Chirp f_{slope}	Sync precision T_{step}	Residue ratio w
$\leq$20 MHz/us	5 ns	50%
$\leq$40 MHz/us	2.5 ns	43%

3.2 Residual decomposition and marginal impact on CE

There is a residual after removal due to the sync precision and nonlinear variations. The residual will be decomposed when the long preamble makes a correlation for the time sync and fine FO estimation; it will also be decomposed when the FFT is performed for frequency-domain equalization. Here, we focus on fine FO estimation for illustration. We use a step-search method, where f_{step} is the step size in the search. $Pr(t)$ is the composite preamble at the transmitter, as shown in Eq. (1). $P_r''(t)$ is the received composite preamble at the receiver after coarse offset correction, and its discrete form is $P_r''(n) = P_r(nT_s)e^{j2\pi f_\Delta nT_s}$. Here, f_Δ denotes the residual fractional offset and $f_\Delta \in [f_{min}, f_{max}]$.

Let $L_{ak}(n) = L_a(n)e^{j2\pi(f_{min}+k\cdot f_{step})nT_s}$, denote multiple different FO local sequences, $k = 0, 1, 2, \dots$. Then,

$$z_k = \sum_{n=1}^{l} P_r''(n) \cdot L_{ak}(n)*$$
$$= \sum_{n=1}^{l-i} L_a(n)e^{j2\pi f_\Delta nT_s} \cdot L_{ak}(n)*$$
$$+ \sum_{n=l-i+1}^{l} (L_a(n) + s(n-l+i))e^{j2\pi f_\Delta nT_s} \cdot L_{ak}(n)$$
$$= \sum_{n=1}^{l} |L_a(n)|^2 \, e^{j2\pi(f_\Delta - f_{min} - kf_{step})nT_s} + \delta \qquad (7)$$

Equation (7) shows that the received composite preamble correlates with the different local FO sequences. l is the sample point number of the entire received long preamble ($P_r''(t)$), and i is the sample number of the composite fragment $[L_a(t) + s(t)]e^{j2\pi f_\Delta nT_s}$. In this paper, $i = 200$; $l = 2560$ when $f_s = 400$ M, $T_{chrp} = 0.5$ us, $T_L = 6.4$ us; see Table 2 in Section 4. When $(f_{min} + k \cdot f_{step}) = f_\Delta$, z_k obtains its maximum value $\sum_{n=1}^{l} |L_a(n)|^2$, and f_Δ can be estimated as $f_\Delta = \underset{k}{\arg\max}(|z_k|) \cdot f_{step} f_{min}$.

Table 2 Integrated signal parameters

	Duration	Period	Average power	T_{step}
Long preamble	$T_L = 2T_{FFT} = $ 6.4 us	$T_{FFT} = 3.2$ us	P_L	$T_{step} = 5$ us
Chirp overlapped	T_{chrp}=0.5 us	a Chirp/preamble	$P_{chrp} = $ 12~2PL	

δ in Eq. (7) determines the influence of the overlap:

$$\delta = \sum_{n=l-i+1}^{l} s[(n-l+i)] \cdot L_a^*(n)$$
$$\leq \sum_{n=l-i+1}^{l} \left| s[(n-l+i)] \cdot L_a(n)^* \right|$$

When $|L_a(n)|$ is a roughly constant envelope, the induced relative error $_\Delta\delta$ can be estimated as

$$\Delta\delta = \frac{\delta}{\sum_{n=1}^{l} |L_a(n)|^2} \leq \frac{\sum_{n=l-i+1}^{l} |s[(n-l+i)T_s] \cdot L_a(n)^*|}{\sum_{n=1}^{l} |L_a(n)|^2}$$
$$\leq \frac{\sum_{n=l-i+1}^{l} |s[(n-l+i)]|}{\sum_{n=1}^{l} |L_a(n)|} \approx \frac{i \cdot \frac{2}{\pi}\sqrt{2\bar{p}_{chrp}}}{l \cdot \sqrt{\bar{P}_L}}$$
$$\leq \frac{i}{l} \cdot \sqrt{\frac{\bar{p}_{chrp}}{\bar{P}_L}} = \frac{T_{chrp}}{T_L} \cdot \sqrt{\frac{\bar{p}_{chrp}}{\bar{P}_L}} \qquad (8)$$

After removal, $_\Delta\delta$ can be estimated as

$$\Delta\delta \leq \frac{T_{chrp}}{T_L} \cdot \sqrt{\frac{\bar{p}_{chrp} \cdot w}{\bar{P}_L}} \qquad (9)$$

where $\bar{p}_L$ and $\bar{p}_{chrp}$ are the average powers of the preamble and chirp, $\frac{2}{\pi}\sqrt{2\bar{p}_{chrp}}$ in Eq. (8) is the mean value of the constant envelope $|Chirp|$, and w is the residue rate.

In this paper, we focus on the influence of the removal and residual on fine FO estimation and equalization. The influence on time sync is relatively small. We also recommend using the composite signal as the long preamble directly for the fine time sync, FDE, etc., therein replacing the original preamble at the Tx side (transmitter) and Rx side (receiver). This is one of the next steps in our research.

3.3 Extracting sensing part for recognition

The composite sensing signal is extracted after the time sync, and the composite signal fragment is used directly for recognition:

$$L_a(t) + s(t) \quad T_L - T_{chrp} < t \leq T_L \qquad (10)$$

Combined with a current recognition algorithm based on UWB or WiFi [9, 28], it can be used to sense the shape and size of an object.

4 Experimental

We first simulate the performance of FO estimation and FDE, and then according to the results, we calculate the effect on RCE. Next, according to Table 90 "Allowed RCE
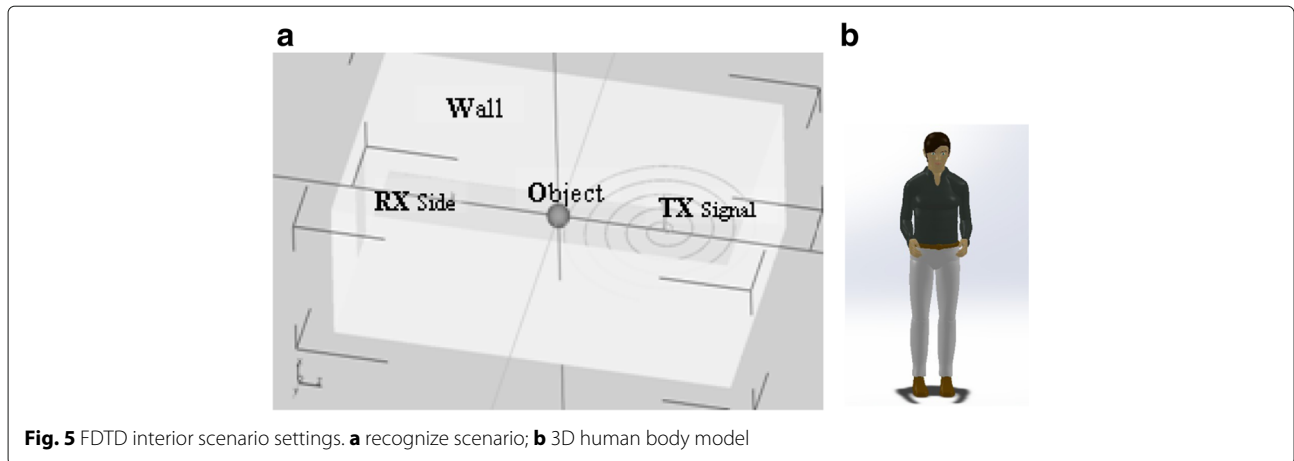
Fig. 5 FDTD interior scenario settings. **a** recognize scenario; **b** 3D human body model

versus data rate" in 802.11a, we obtain the allowed rate under different RCE and make an evaluation of the transmission. Finally, we test out the target recognition by using the preamble signal.

4.1 Frequency offset estimate

Fine FO estimation and FDE are the main functions of the long preamble. Impacting on FO estimation due to the composition will increase rotation error of the constellation. So in this section, we simulate FO estimation by using composite preamble, and Fig. 4 is drawn. Then, according to the result, we calculate the effect on RCE. To consider the influence on fine FO estimation, we use MATLAB 2014a; And in the next two sections, we use the eastwave FDTD electromagnetic platform.

802.11a [18] is the reference for the simulation parameters. The long preamble La is the IFFT of $L = \{000000, L_{-26,26}, 00000\}$, where $L_{-26,26} = \{1, 1, -1, \ldots, -1, 1, 1, 1, 1\}$, and long preamble includes two L periods $2T_{\text{FFT}}$. On the Rx side, it correlates with the local sequences for fine FO estimation based on a step-search method, and the coarse offset has been corrected based on the short preamble. And we set front-end sample rate $f_s = 400$ MHz, $T_{\text{step}} = 2T_s = 5$ ns, the power of the overlapped chirp P_{chrp} is 1.2 to 2 times the long preamble P_L.

For the reason that the increase in the error rate is not noticeable when the FO error $\epsilon_f < 10$ kHz [29], we set $f_{step} = 6.4$ kHz. In this way if the FO estimation falls in the correct interval, ϵ_f will be 3.2 kHz, which meets the requirement of $\epsilon_f < 10$ kHz. Even if the estimated results fall in the adjacent area, $\epsilon_f < 6.4$ kHz only slightly increase the rotation error of constellation, will not affect the follow-up equalization estimation (see Fig. 7 and relevant explanation in 1st paragraph of Section 4.2.3). See Table 2 for the other parameters.

Figure 4 is the result of FO estimation using composite preamble vs.original preamble. Figure 4a shows

that the FO estimation accuracy is decreased by approximately 3–4% under high-signal-to-noise-ratio (SNR) conditions after overlap and removal, and the accuracy is greater than only de-spreading is performed [16]. And as a result of $\Delta f \cdot t = \Delta \phi$, FO estimation error Δf will increase the rotation error of the constellation($\Delta \phi$).When $\Delta \phi$ is very small, $\Delta r/r \approx sin\Delta \phi \approx \Delta \phi$ (see the small graph inserted in Fig. 4, $\alpha \approx 90°$ there), here r is magnitude of the point in constellation, Δr is magnitude of the constellation error.Hence,it can be considered that the 3-4-% Δf error leads to the corresponding increase in RCE. And since the small increase of ϵ_f does not affect the completion of the following FDE, we can add together the RCE increase derived in this section and the increase derived in next section, then we get the total RCE increase, no more consideration of mutual influence.

Figure 4b shows the f_Δ accuracy curve with chirps at varying powers, where the power is easy to adjust according to the estimation and recognition precision. The curves are flatted at high SNR, with a flooring effect being exhibited [30]. This shows that to further improve estimation and recognition concurrently, we must improve the removal effect.
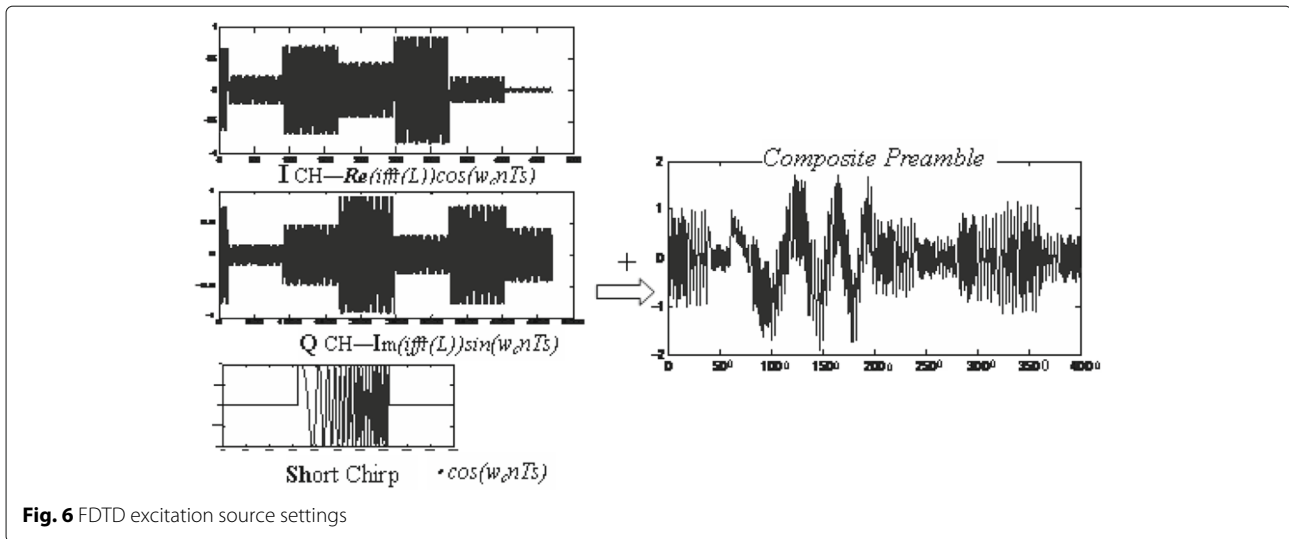
4.2 Frequency-domain equalization

4.2.1 FDTD scenario and calculation settings

The FDTD simulation provides greater accuracy than the general multi-path model [31]. We use the eastwave
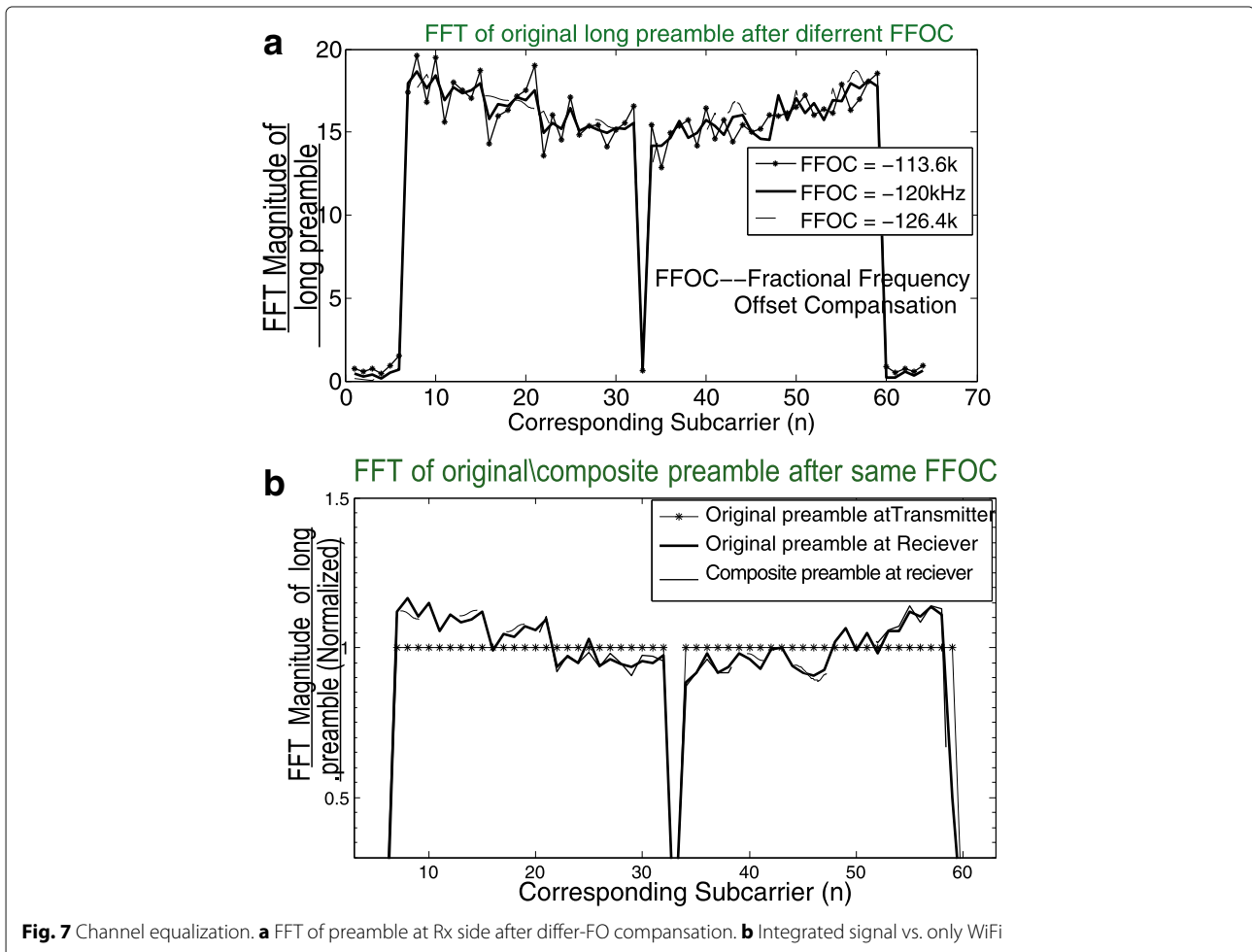
Table 3 FDTD calculation settings

Carrier frequency	5.2 GHz	Duration	3.2 us
Bandwidth	20 MHz	FDTD Tstep	8e−12 s
Frequency interval	0.3125 MHz	spatial Grid	50x150x300
Total steps	4e5	y, z boundary	PML absorb
Recording rate	400 MHz	X boundary	Periodic PML=6

Zheng *et al. EURASIP Journal on Wireless Communications and Networking* (2018) 2018:215

Page 8 of 12

Fig. 6 FDTD excitation source settings

FDTD simulation platform, which is China's first parallel all-vector electromagnetic simulation platform. The platform is based on a strict FDTD and physical optics model; its calculation speed is 10 to 100 times higher than similar algorithms found worldwide. The parameters

of the FDTD simulation were set as 2.9×1.5×2 m based on our lab, where the distance between the RX and TX antennas is 1.6 m and the length of an antenna is 12 cm. The sensed object is placed in the middle. Figure 5 shows the FDTD scenario.

Fig. 7 Channel equalization. **a** FFT of preamble at Rx side after differ-FO compansation. **b** Integrated signal vs. only WiFi

The wall of the lab is composed of ground glass, and its reflectivity is always large; therefore, the absorption boundary's perfectly matched layer (PML) is set to 6 [26]. See Table 3 for other FDTD calculation parameters.

4.2.2 FDTD signal settings

Referring to 802.11a and the overlapping scheme in Fig. 1, we set our FDTD excitation source as shown in Fig. 6. The data of the FDTD recorder is output to Matlab2014 for data processing. Under 802.11a, $L_a(t) = w_{\mathrm{Tlong}}(t) \sum_{k=-26}^{26} L_k \exp\left(j2\pi k\Delta_F(t - T_{G12})\right)$, where $w_{\mathrm{Tlong}}(t)$ is the time window and T_{G12} is the guard interval. The discrete form of the long preamble is $La(k) = w_{\mathrm{Tlong}}(k) \cdot IDFT_{64}(L)$, and

$$w_{\mathrm{Tlong}}(k) = \begin{cases} 1 & 1 \le k \le 62 \\ 0.5 & k = 0, 63 \end{cases}$$

The RF signal is $r_{RF}(t) = Re(r(t)) \cdot cos(w_c t) - Im(r(t)) \cdot sin(w_c t)$ [18]; thus, the I channel is endowed with $Re[ifft(L)]$, and the Q channel is endowed with $Im[ifft(L)]$. Then, we obtain the integrated signal as shown in Fig. 6.

4.2.3 Equalization results

Figure 7a is the FFT of the received preamble under varying fractional frequency offset compensations (FFOC). The figure shows that the preamble can achieve FDE even when fractional FO estimated value f_Δ has a slight error (When f_Δ has a slight error such as ϵ_f=6.4kHz here, the FFOC will change as well, and then the curve is slightly different.However,the FDE can still be achieved). [29] also indicates that f_Δ is allowed a certain error. In addition, from the perspective of the sum of squared deviations (SSD), the line is flattest when FFOC = -120 kHz, and thus, -120 kHz may provide the best performance. SSD is defined as $\sum_{n=1}^{64} [d_n - E(d)]^2$, where d indicates the curve and $E(d)$ is its mean value.

Figure 7b shows the FFT of the WiFi preamble (solid line s_n) and the FFT of the composite preamble after removal on the Rx side (dotted line d_n) after compensation at -120 kHz. m_n(marked line) is WiFi at the transmitter. Thus, $s_n - m_n$ is the equalization coefficient, and $d_n - s_n$ is the equalization error due to the residual. We defined the relative equalization error:

$$\sqrt{\Sigma \left[d_n - s_n\right]^2 / \Sigma \left[s_n - m_n\right]^2} = \Delta J \qquad n = 1, 2, 3 \ldots, 64 \tag{11}$$

By computation, $\Delta J = 9.5\%$ slightly increases RCE, and taking into account the 3% increase in phase rotation RCE caused by the fre-offset error mentioned in Section 4.1, it will lead to an increase in the RCE from -25 dB to -16 dB or -19 dB to -13 dB. Accordingly, the data rate decreases from 54 Mbps to 24 Mbps or 36 Mbps to 18 Mbps (Table 4).

Table 4 Equalization error leads to a fractional increase in RCE

Corresponding data rate of 802.11a	Relative constellation error (dB)
6M\9M	-5\-8
12M\18M	-10\-13
24M\36M	-16\-19
48M\54M	-22\-25

(if the sync precision improves to $T_{step} = 2.5$ ns, the data rate decreases from 54 Mbps to approximately 48 Mbps)

4.2.4 Assessment of the communication

According to the test results,analytical,calculation in 4.1 and 4.2.3: FO estimation error increases the rotation error of constellation, equalizing compensation error causes the diffusion of constellations. Combining the results of the two, the total RCE increase due to the composition is got. And then according to Table90 in 802.11a (Table 4 in this paper), we obtain the allowed rate under different RCE, Table 5 is got and Fig. 8 is drawn.

Table 5 shows the Rb_{max} comparison of some super-resolution design methods occupying the same 20 MHz of bandwidth, except the time-division integration [1] is 100 MHz of bandwidth.

Figure 8 shows the assessment of the communication capability compared to time-division (TD) multiplex integration when they are applied to the same OFDM modulation based on 802.11a. Here, communication duty ratio (C duty ratio) is the communication proportion under TD multiplex integration. For TD integration mode, with the increase of the C duty ratio, its transmission capacity increases;and when C duty ratio is from 2/3 to 3/4, or from 3/4 to 4/5..., the increase is getting slower. The data rate of composition mode is not very different from the TD mode when C duty ratio of the TD mode is more than 3/4. In addition, composition mode has certain advantage when RCE is less than -22 db, and then we say that it has a high transmission capacity.

4.3 High-resolution recognition

We use the output of the FDTD simulation in Section 4.2 to compare the recognition effect of only using WiFi and when using the composite signal. Two groups of experiments were performed. One group attempts to distinguish

Table 5 Rb_{max} Performance comparison

Integration method	Rb_{max}
Composition in this study	24 M/48 Mbps
20M pulse OFDM [11]	5.4 Mbps
20M continuous LFM-MSK [9]	916 k/1.6 M
100M time-division [2]	about 50 Mbps

Zheng *et al. EURASIP Journal on Wireless Communications and Networking* (2018) 2018:215

Page 10 of 12

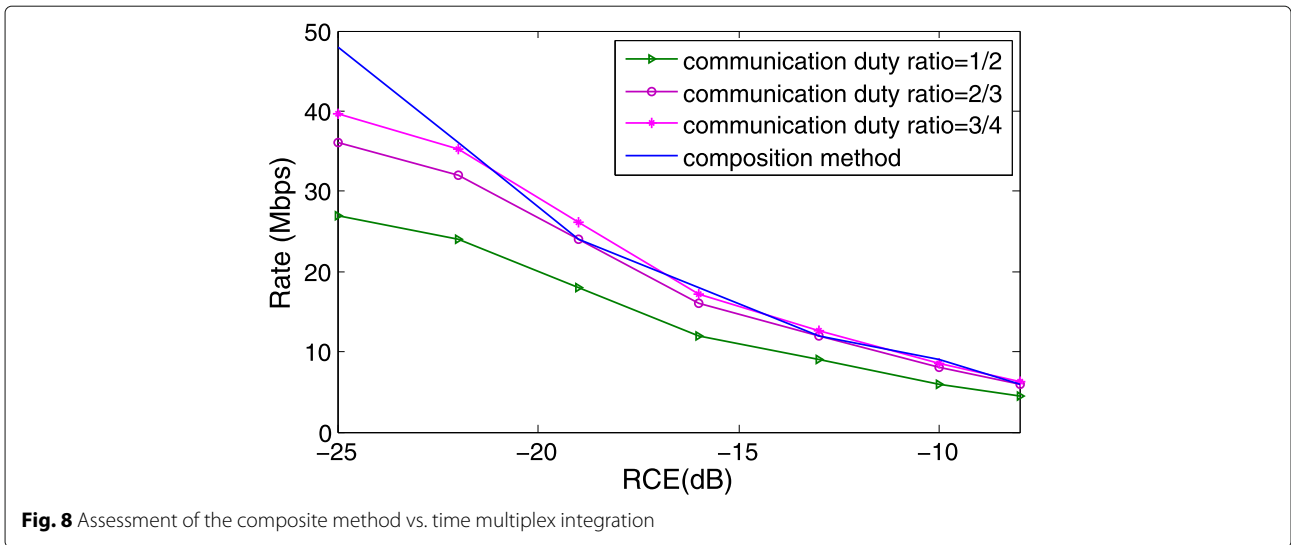**Fig. 8** Assessment of the composite method vs. time multiplex integration

between a basketball (Φ25 cm) and a volleyball (Φ21 cm); the other group attempts to distinguish between a football (Φ22 cm) and a volleyball. Besides identifying balls with different diameters,we also added a human standing/lying recognition simulation. The height of the 3D human body model is set to 1.55 m(see Fig. 5b), and the simulation result is drawn in Fig. 5b.

Based on the normalization of the long preamble, time-domain features of the composite signal fragment were extracted, including the energy, excess delay, rms delay, maximum value, standard deviation, and peak value. The SVM classifier *svmtrain* and the *svmpredict* function in MATLAB2014 were used in both experiments. A radial basis kernel was used, and the parameters *c* and *g* were set to 1 and 10, respectively. A total of 600 training samples and 1400 test samples for each ball were selected. ϵ_r of the

ball was set to 3, and the porosity was set to 0.97. The wall of the lab is composed of ground glass, so our absorption boundary PML is set to 6.

Figure 9a is the identification results of the basketball and volleyball; if test_data of the basketball is input into the SVM model and the output is basketball, the result is recorded as being correct. The solid line indicates the correct recognition rate of the basketball, and the dashed line indicates the correct recognition rate of the volleyball. Figure 10 is the result for the football/volleyball. And Fig. 9b is the result for human standing/lying.

Figure 9a shows that under the same SNR conditions, the composite signal achieves a higher correctness. The resolution enhancement is slightly when $1.2P_L$chirp is overlapped; the enhancement is further obvious when $2P_L$chirp is overlapped. However, the
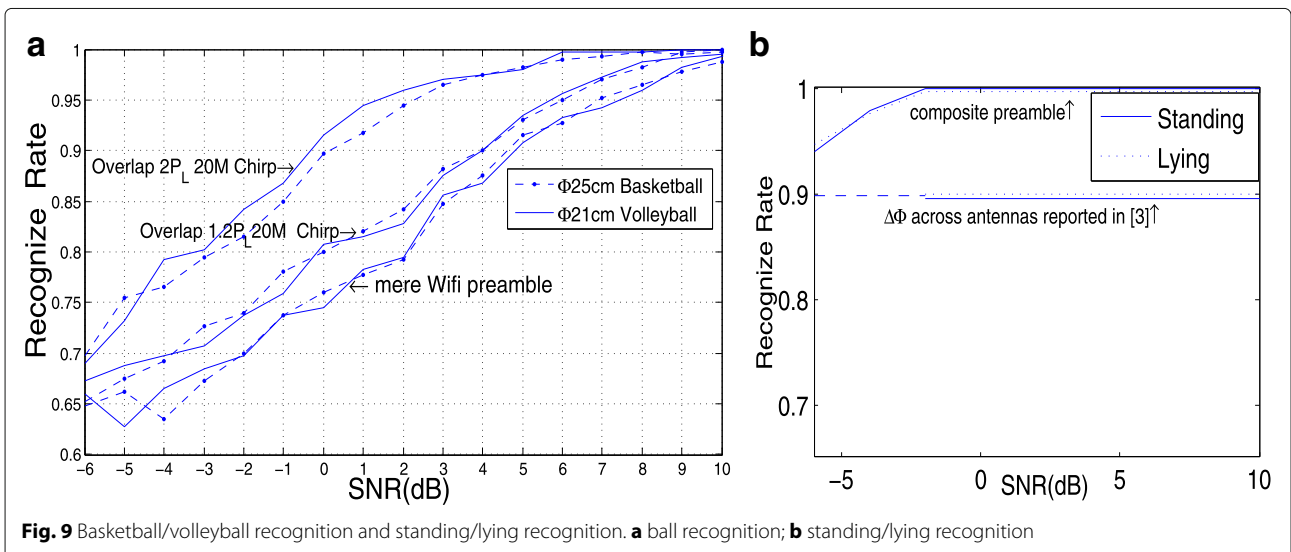

Fig. 9 Basketball/volleyball recognition and standing/lying recognition. **a** ball recognition; **b** standing/lying recognition
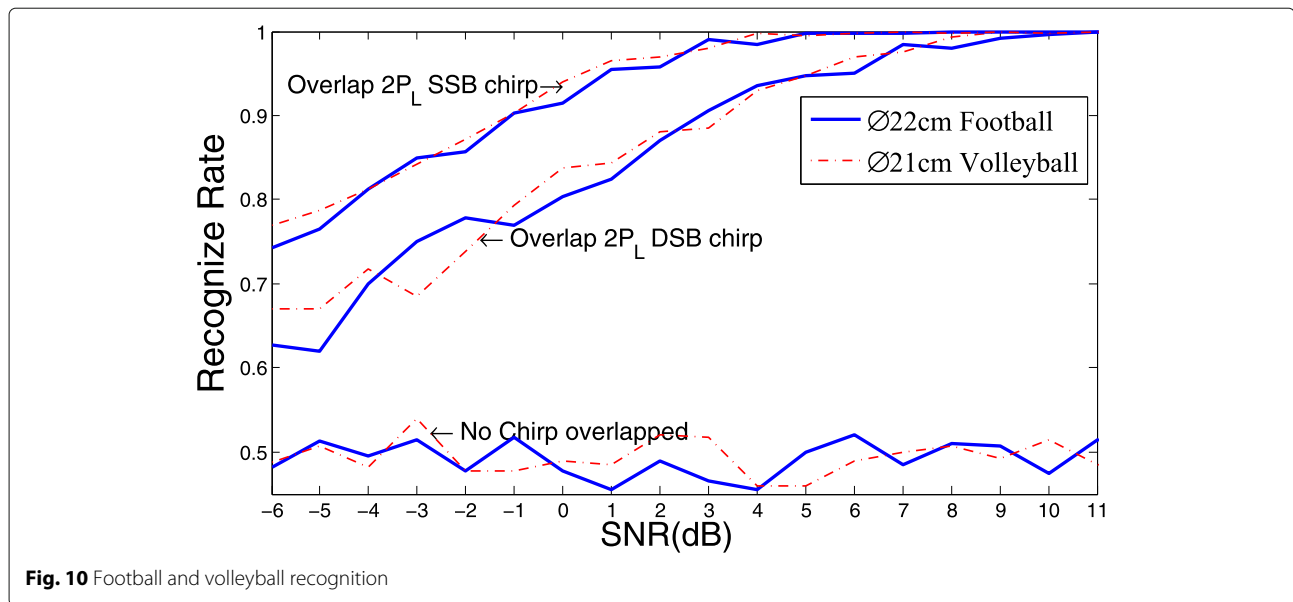
Fig. 10 Football and volleyball recognition

impact on channel estimation requires extreme control, so there is a certain restriction on the power of chirp and the enhancement has a certain limited. In Fig. 10, the recognition effect is enhanced more clearly when difference between the objects becomes smaller,the recognition cannot be done by using original WiFi. Figure 10 also shows that under the same power and bandwidth, overlapping SSB signal is more efficient. The method is useful for interior target recognition, such as Fig. 9b shows nearly 100% standing/lying recognition accuracy in our simulation when preamble signal was used.

5 Conclusions
In this paper, an overlapped composition method is studied to improve the recognition resolution of WiFi signals. A separation method based on cancelation and decomposition is also studied. The power of the overlapping signal can be easily adjusted according to the sensing resolution and CE precision. The FDTD simulation shows that the composite signal achieves a better target recognition resolution than using the WiFi preamble alone. In addition, the method has a relatively high communication capacity.

For future work, we would consider whether a suitable composite sequence can be used to replace the original preamble at both Tx and Rx sides, and the sequence is used for recognition and CE directly. Such as we may research F-domain composition or convolution next, there would then be no need to consider the effects of deletion and residues, so the power of chirp can be increased much more.

Authors' contributions
This work was conducted by ZXK as part of his Ph.D. studies. He was advised by Professor Tj. All authors read and approved the final manuscript.

Authors' information
Xiaokun Zheng was born in Baoding city, China, in 1962. He received his B.S. and M.S. degrees from Northwestern Polytechnical University, Xi'an in 2001. In addition, since 2012, he has embarked on his Ph.D. degree from Beijing University of Posts and Telecommunications. Since 2003, he has been a lecturer at the College of Electronics, Hebei University. His research interests include short-range wireless communication and wireless sensor networks. Prof. Ting Jiang was born in Weiyuan city, Sichuan Province in 1962. He received his Ph.D. degree from Yanshan University, Qinhuangdao, in 2003. Since 2009, he has been a Professor with the Key Labs of Universal Wireless Communications, Beijing University of Posts and Telecommunications. His research interests include wireless broadband interconnection, short-distance wireless communication technologies, and wireless sensor networks. He hosted two National Science Foundation projects, 1 National Major Technical Project and many enterprise projects. Xue Wenling was born in Baoding, Hebei Province, China, in 1975. She received her B.S degree in Computer Applications from Hebei University, Baoding, China, in 2001. She is currently a PhD student at Key Laboratory of Universal Wireless Communications, Beijing University of Posts and Telecommunication, Beijing, China. Her research interests include target detection and classification and signal processing.

References

1. H. Liang, W. Ke, 24-GHz integrated radio and radar system capable of time-agile wireless communication and sensing. IEEE Trans. Microw. Theory Tech. **60**(3), 619–31 (2012)
2. A. Farina, Guest editorial: special issue on bistatic and MIMO radars and their applications in surveillance and remote sensing. IET Radar Sonar Navig. **8**(2), 73–4 (2014)
3. C. C. Hongbo Jiang, Smart home based on WiFi sensing: A survey. Dig. Antennas Propag. Soc. Int. Symp. **6**, 13317–25 (2018)
4. F. Adib, D. Katabi, See through walls with WiFi!. ACM SIGCOMM. **43**(4), 75–86 (2013)
5. Q. Pu, S. Gollakota, S. Gupta, in *Proceedings of the 19th Annual International Conference on Mobile Computing & Networking. ACM*. Whole-home gesture recognition using wireless signals (ACM Mobi Com, 2013), pp. 27–38
6. T. H. Tegan Webster, Passive multistatic radar experiment using WiMAX signals of opportunity. part 2: Multistatic velocity backprojection. IET Radar Sonar Navig. **10**(2), 248–55 (2016)
7. H. X. Yu Guo, Learning using privileged information for HRRP-based radar target recognition. IET Sign. Process. **12**(2), 188–97 (2018)
8. Z. K. Usman Mahmood, *A deep learning framework using passive WiFi sensing for respiration monitoring*. (IEEE GLOBECOM, 2017), pp. 1–6
9. Y. Zhong, T. Jiang, Z. Zhou, in *IEEE ICC Workshop on Radar and Sonar Networks*. A novel gesture recognition method by Wi-Fi communication signal based on fourth-order cumulants (IEEE ICCW, London, 2015), pp. 10567–10571
10. L. Zhipeng, *Waveform research on integration of radar and communication. PhD thesis*. (Beijing Institute of Technology, China, 2015)
11. L. Yongjun, A super-resolution design method for integration of OFDM radar and communication. J. Electron. Inf. Technol. **38**(2), 425–33 (2016)
12. A. K. Mishra, M. Inggs, in *IEEE Electronics, Computing and Communication Technologies ,Bangalore*. FOPEN capabilities of commensal radars based on whitespace communication systems (IEEE CONECCT, Bangalore, 2014), pp. 1–5
13. H. Takase, M. Shinriki, in *15th International, Radar Symposium (IRS)*. A dual-use radar and communication system with complete complementary codes (IEEE IRS, Gdansk, 2014), pp. 16–47
14. S. Sen, OFDM radar space-time adaptive processing by exploiting spatio-temporal sparsity. IEEE Trans. Sign. Process. **61**(1), 118–30 (2013)
15. L SY, in *IEEE Radar Conference, Cincinnati*. MIMO OFDM radar with communication and interference cancellation features, (2014), pp. 19–23
16. E. R. B. Mark Roberton, *Integrated radar and communication based on chirp spread-spectrum techniques*. (IEEE, Philadelphia, 2003), pp. 611–614
17. Z. Tianxian, X. Xianggen, OFDM synthetic aperture radar imaging with sufficient cyclic prefix. IEEE Trans. Geosci. Remote Sens. **53**(1), 394–404 (2015)
18. IEEE standard 802.11a Part 11, Wireless LAN medium access control MAC and physical layer (PHY) specifications (1999)
19. C. Knapp, G. Carter, The generalized correlation method for estimation of time delay. IEEE Trans. Acoust. Speech Signal Process. **24**(4), 320–7 (1976)
20. Z. X. Liang Ruihai, Design and implementation of real-time estimator of time difference of arrival based on parallel correlation. Application of Electronic Technique. **37**(2), 91–94 (2011). https://doi.org/10.16157/j.issn.0258-7998.2011.02.043
21. R. D. A Gusmao, N. Esteves, On frequency domain equalization and diversity combining for broadband wireless communications. IEEE Trans. Commun. **51**(7), 1029–33 (2003)
22. J. D. S. Iker Sobron, Device-free people counting in IoT environments: new insights, results and open challenges. IEEE Internet Things J. **PP**(99), 1–6 (2018)
23. F. A. Hamza, The USRP Under 1.5X Magnifying Lens. https://www.gnuradio.org/doc/doxygen/index.html
24. H. Minsheng, Computation of the ambiguity function of PD radar. Informatization Res. **35**(2), 22–25 (2009)
25. T. J. P. SG Glisic, New PN code acquisition scheme for CDMA networks with low signal-to-noise ratios. IEEE Trans. Microw. Theory Tech. **47**(2), 300–10 (1999)
26. T. Ohtani, A stability improvement technique using PML condition for the three-dimensional nonuniform mesh nonstandard FDTD method. IEEE Trans. Magn. **May**, 1569–72 (2013)
27. G. S. S. G Maloney, in *Digest on Antennas and Propagation Society International Symposium*. Accurate computation of the radiation from simple antennas using the finite-difference time-domain method (IEEE San Jose, CA, 1989), pp. 42–45
28. T. J. Zhou Ge, in *IEEE Global Conference on Signal and Information Processing (Global SIP)*. A new method of dynamic gesture recognition using Wi-Fi signals based on DWT and SVM improved by DTW, (2015), pp. 1214–1218
29. L. X. Li Shuo, Research on 802.11a frequency deviation measurement. Application of Electronic Technique. **31**(5), 48–50 (2005)
30. Z. k. Wangwen Bo, *Wideband wireless communication OFDM technology*. (Posts&Telecom Press, Beijing, 2003)
31. W. Yang, Multipath model for UWB indoor Los environments. J. Commun. **26**(10), 24–28 (2005)